PHYSICAL REVIEW B **91**, 125116 (2015)

Quasiparticle self-consistent *GW* calculations of the electronic band structure of bulk and monolayer V_2O_5

Churna Bhandari and Walter R. L. Lambrecht
Department of Physics, Case Western Reserve University, Cleveland, Ohio 44106-7079, USA

Mark van Schilfgaarde
Department of Physics, King's College London, London WC2R 2LS, United Kingdom

(Received 24 September 2014; revised manuscript received 27 January 2015; published 10 March 2015)

Quasiparticle self-consistent (QS) *GW* calculations are performed for bulk and monolayer V_2O_5. The orbital character of the bands and the bulk monolayer difference at the LDA level are discussed first. We find that the QS*GW* self-energy overestimates the gap by an unusually large amount. The main reason for this is identified to be the lattice polarization effect: The large LO-TO splittings in this polar material enhance the screening and reduce the screened Coulomb interaction affecting the gap. The effect is estimated to reduce the screened Coulomb interaction and hence the self-energy by a factor 0.38 (for bulk) and brings the calculated optical response functions in fairly good agreement with experiment. For monolayer V_2O_5 we find that the QS*GW* gap varies as $1/L$ with L the size of the spacing between the monolayers in a supercell. This results from the long-range nature of the self-energy $\Sigma = iGW$ and the similar $1/L$ behavior of the dielectric screening.

DOI: 10.1103/PhysRevB.91.125116 PACS number(s): 71.20.Ps, 73.21.−b

I. INTRODUCTION

Since the Nobel prize winning work of Novoselov and Geim [1], two-dimensional materials such as graphene and transition metal dichalcogenides (TMDC) have attracted a great deal of attention because of their unique electronic, optical, and transport properties. The exfoliation technique applied first to graphene has opened a path to the investigation of other materials in ultrathin monolayer or few monolayer form. Other techniques for deposition of ultrathin layers over larger areas have subsequently been developed. In spite of the already weak bonding between the layers in their bulk form of these materials, surprisingly different properties were discovered for the few-layer forms of these materials. Most of these materials currently studied share a hexagonal network structure.

Vanadium pentoxide (V_2O_5) is another and rather different layered material. Its crystal structure also consists of weakly bonded layers but has orthorhombic symmetry, and, in addition, it has certain one-dimensional (1D) structural aspects [2]. It consists of zigzag double chains bonded together with bridge oxygens. The crystal structure is shown in Fig. 1. The structure can be viewed as consisting of chains of square-based pyramids of five oxygens surrounding each V, which point alternately up and down and share an edge along the chain direction. These double chains are connected via a corner shared bridge oxygen. There are hence three structurally different types of oxygen in this structure: the vanadyl oxygen (O_v) is bonded to a single vanadium and forms the apex of the pyramids; the bridge oxygen (O_b) is bonded to two vanadiums and couples the chains together, while the chain oxygen (O_c) binds to three vanadiums, two along the chain direction and one in the adjacent chain. They form the shared edge between the pyramids in the double chain. It is thus of interest how this 1D character will manifest itself in the electronic and transport properties of the material.

Electronically, V_2O_5 appears at first sight simple because it has a filled oxygen valence band and empty vanadium d-like conduction bands and should thus be a wide gap insulator. However, already in the early band-structure calculations [3,4] it was found that there is a split-off conduction band, resulting from the d_{xy} orbitals. More precisely, the four V d_{xy} orbitals per cell form four bands, two of which are antisymmetric with respect to the mirror plane passing through the bridge oxygen. This prevents π-like interaction with the bridge oxygen p_y orbital (along the chain direction) and hence separates this band from the higher lying V d orbitals which all have some π- or σ-antibonding character with O p. This split-off band has significant dispersion only along the chain direction and thus manifests the 1D character of the material. Tight-binding parametrizations of these bands are discussed for example in Smolinski *et al.* [5]. The orbital character of the bands will be reviewed in the present paper in Sec. III A.

This separated narrow d band with 1D dispersion has important consequences in doped V_2O_5. Doping can for instance result from oxygen vacancies. In fact, the vanadyl oxygen, which is singly bonded to V, can easily be removed in reducing chemical environments and leads to a series of (ordered) lower oxides, V_4O_9, V_6O_{13}, etc. [6]. On the other hand, it is responsible for the catalytic activity of V_2O_5 in oxidation reactions, which forms one of the main industrial applications of this material [7]. Besides influencing the conductivity of the material, which shows a variable range hopping conductivity [8], this type of doping also leads to optical transitions in the infrared between the split-off band and the higher conduction bands [9].

Another route to doping this split-off band is via intercalation. This leads to the so-called V_2O_5 bronzes. These have attracted significant attention because of their interesting 1D magnetic properties. The intercalates reside in between the layers in the large interstitial site in between the bridge oxygens. For a monovalent dopant of one atom per V_2O_5 unit, as in Na_2O_5, the split-off band is exactly half-filled. Because of the strong Coulomb interaction in a narrow band, this corresponds to a 1D half-filled Hubbard model. Actually, viewed

 ©2015 American Physical Society

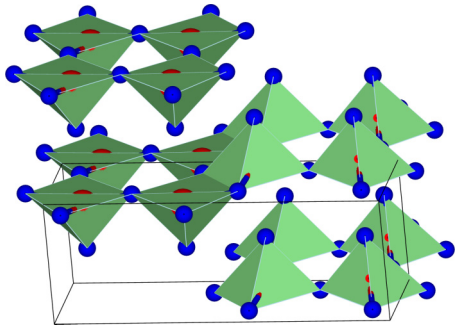

FIG. 1. (Color online) Crystal structure of V_2O_5: large red spheres inside the nearest neighbor coordination pyramids represent V, small blue ones represent O.

with respect to the four bands formed from the d_{xy} orbitals it corresponds to one quarter filling. A spin-Peierls transition was observed for this material by Isobe and Ueda [10] in 1996 and has since then attracted great attention [5,11–14]. At that time it was believed that there was a charge disproportional between the V in the up and down pointing pyramids, leading to alternating V^{4+} and V^{5+} chains with the spin-Peierls transition taking place in the V^{4+} chain. Later it was found [5] that the V atoms in this structure all stay equivalent and should be viewed as $V^{4.5}$. The states in the lowest band can be viewed as V-V bonding molecular states in the V-O_b-V units. These are then viewed as rungs in a ladder and these materials are hence called ladder compounds. Although the band made from the bonding states in the rung is half-filled, the overall system of the ladder compound including the corresponding antibonding states (higher band) is quarter-filled. The nature of the transition at low temperature is still controversial and may be a charge-ordering rather than a spin-Peierls transition or two transitions very close to each other.

Antiferromagnetic ordering of the spins along the y direction would lead to a doubling of the periodicity along the chain. However, for 1D systems, strict ordering is not expected and, instead, the possibility of separated charge and spin excitations has been predicted [15]. The weak coupling between these chains makes this system intriguing because they are in between strict 1D and two-dimensional (2D) systems. It is these features which have generated the interest in such systems from a many-body theory point of view. It is believed to be the origin of the above mentioned phase transition although the exact nature of the structure below the critical temperature has not yet been determined, to the best of our knowledge. For example, it is not clear if it is accompanied by a structural bond-length alternation. Band structure calculations [13,14] in LDA + U predict formation of magnetic moments and a gap opening in the split-off band in an antiferromagnetically ordered state. Meanwhile, in divalent atom intercalated bronzes, such as MgV_2O_5, interesting spin wave excitations have also been observed [16].

Our renewed interest in this material results from the observation that for ultrathin few monolayer systems, the possibility exists of injecting electrons in this split-off band by means of gating. Therefore, monolayer or few-layer versions of V_2O_5 could provide a more systematic control of the doping of this 1D band. Another interesting possibility is that by removing rows of bridge oxygens, one could form nanoribbons of monolayer V_2O_5. The edges of these would present additional modifications of the orbital character of the split-off bands but would also essentially dope the system with electrons. A variety of nanoforms of V_2O_5 have already been observed [17–22], but a systematic understanding of their electronic properties is still lacking. In a previous paper [23] we studied the differences between bulk and monolayer on the phonons in V_2O_5 and found important changes due to the differences in screening.

As discussed above, interesting strongly correlated physics has already been studied extensively in bulk forms of this material and has focused on the correlation effects within the doped 1D split-off band. However, until now the many-body effects on the band gap and overall electronic structure have received little attention and also the monolayer versus bulk changes in the electronic structure have not been systematically studied.

While several previous first-principles band structure studies have been performed [24–27] of this material in the local density approximation (LDA) or generalized gradient approximation (GGA), these methods suffer from underestimates of the band gap. We are aware of only one previous study of V_2O_5 band structure at the GW level [28]. A few studies also considered monolayers or surfaces [25,27], but no dramatic changes were found. For example, the gap stayed indirect and modest changes in the band gap were found. It has been found, in previous work on transition metal dichalcogenides, that much stronger effects result from the 2D character in GW calculations because of the important changes in 2D screening and the long-range effects in GW [29]. Reduced screening effects were already manifested in monolayer V_2O_5 to have an effect on the phonons [23].

Here we present quasiparticle self-consistent (QS) GW calculations [30] of the pure and undoped V_2O_5 band structure to test how well this method describes a strongly correlated 2D material. A study of doped V_2O_5 is postponed for future work. We find that the band gap in bulk is significantly overestimated by this method. The QSGW is known to systematically overestimate the gap in most materials and this is usually attributed to the underscreening of the random phase approximation in the GW method. In other words, W is overestimated by the lack of electron-hole interactions. In the present material, the overestimate is found to be unusually large and thus we need to look for additional effects. We analyze the optical data on the band gap and conclude that the reason for the discrepancy is not simply because of the omission of excitons in the GW calculation. In view of the large LO-TO splittings in this polar material, we estimate the effects of lattice polarization on the dielectric constant and hence indirectly on the electron-electron interaction screening and the gap [31,32]. We find this to be the major reason for the discrepancy. An additional correction of W due to missing electron-hole interactions may be expected.

We then apply the same approach to monolayer V_2O_5. After analyzing the changes at the LDA level, we show that at the QSGW level the gap changes depend significantly on the size of the vacuum region used to separate the layers. This observation is similar to what was found earlier in TMDC compounds and reflects the long-range nature of the GW self-energy and the importance of screening in the latter. To show this we demonstrate a $1/L$ dependence of both the gap

and the dielectric constant on the size of the cell in the direction perpendicular to the layers. The lattice polarization reduction factor needs to be included also for the monolayer but it also depends on the layer separation.

The paper is organized as follows. Section II provides the necessary details on the computational approach and Sec. III presents our results. In Sec. III A we first present the LDA bulk and monolayer band differences and explain some of the features already mentioned in this Introduction. In Sec. III B we discuss the bulk QSGW results and their shortcomings. As part of this we discuss the optical data. In Sec. III C we discuss the monolayer band gaps dependence on the interlayer spacing and its relation to the reduced screening.

II. COMPUTATIONAL METHOD

The full-potential linearized muffin-tin orbital method [33,34] was used to solve the density functional Kohn-Sham equations in the local density approximation (LDA) [35,36] and the quasiparticle self-consistent GW equations. The LMTO and GW codes used are available in Refs. [37,38]. The lattice constants were set to the experimental ones to avoid the typical underestimate of the unit cell volume by LDA and the additional problem here of determining the optimal interplanar spacing for a system with weak van der Waals interactions. The internal positions of the atoms, however, were relaxed in the LDA using a conjugate gradient method. They were found to be in good agreement with experiments as can be seen in Table I. No significant changes in the bond lengths were found for the monolayer. The monolayer is studied in a periodic cell simply by increasing the layer separation. The convergence of the monolayer GW calculations with layer separation distance will be discussed in Sec. III C. The monolayer unit cell lattice constant in the direction perpendicular to the layer is denoted by L.

Convergence tests were carried out for the **k**-point Brillouin-zone sampling for the self-consistent calculations as well as for the QSGW self-energy calculations. An unshifted mesh of $2\times6\times6$ for bulk and $2\times6\times1$ for the monolayer were found to be adequate for both purposes. The ratios of the number of divisions along the crystallographic directions was chosen roughly in proportion to their size in the reciprocal lattice. The LMTO basis set includes two sets of $\kappa, R_{\rm sm}$ values, representing the smoothed Hankel function envelope functions decay length ($\kappa^2=\epsilon-v_{mtz}$) and smoothing radii ($R_{\rm sm}$), which modify the orbital curvature of the radial basis function near the muffin-tin radius. For vanadium we used an (spd,spd) and for oxygen an (spd,sp) spherical harmonic basis set. Augmentation of the orbitals inside the muffin-tin spheres includes spherical harmonics times solutions of the radial Schrödinger equation, ϕ and $\dot{\phi}$ (energy derivative) functions up to $l_{\rm max}=4$. In addition, we added V-3p local orbitals.

TABLE I. Bond lengths of GW in Å.

	V-O_v	V-O_b	V-O_{cy}	V-O_{cx}
Calc.	1.55	1.77	1.87	1.97
Expt.	1.585	1.77	1.88	2.02

The QSGW method has been described in detail in Refs. [30,39,40]. Briefly the noninteracting Hamiltonian H^0 for the GW self-energy calculation [41], i.e., the Hamiltonian from which the Green's function G^0 and $W^0=(1-v\Pi^0)^{-1}v$ with v the bare Coulomb interaction and $\Pi^0=-iG^0G^0$ the bare polarization propagator are constructed, includes a nonlocal but energy independent Hermitian exchange correlation potential $[V_{\rm xc}^{\rm QSGW}]_{ij}={\rm Re}\{\Sigma_{ij}(\omega_i)+\Sigma_{ij}(\omega_j)\}/2$ extracted from the previous self-energy ($\Sigma=iG^0W^0$) in an iterative procedure, starting with the LDA potential. The equations above are only written schematically, omitting the coordinate and energy dependencies and integral equation nature of the equations. These quantities are represented in the basis of the H^0 eigenstates labeled i,j. The noninteracting Hamiltonian is thus chosen optimally in the sense that the perturbation becomes as small as possible and the real parts of the quasiparticle eigenvalues converge to the Kohn-Sham eigenvalues of the H^0. Adding the $V_{\rm xc}^{\rm QSGW}$ off-diagonal elements allows mixing between different H^0 eigenstates. Above a certain energy, chosen here to be 2.5 Ry, the $[V_{\rm xc}^{\rm QSGW}-V_{\rm xc}^{\rm LDA}]_{ij}\approx\delta_{ij}(a+\epsilon_i b)$ is restricted to be diagonal and its orbital dependence is assumed to be linear in the orbital energy [40]. A mixed interstitial plane wave plus LMTO product basis set is used [42] as an auxiliary basis set to represent all two-point quantities v, W, Π^0, ε. An important characteristic of this GW implementation is that the self-energy, or rather the $V_{\rm xc}^{\rm QSGW}$, can be expressed in the basis set of real-space muffin-tin orbitals. It can then be determined by Bloch summation for any arbitrary **k** point and hence eigenvalues of the converged $H^{0-{\rm QS}GW}$ can be obtained along symmetry lines from knowledge of the $\Sigma(\mathbf{k},\omega)$ on a small **k**-point mesh set. This constitutes an effective interpolation scheme in **k** space. For clarity, the band structures presented below are the real Kohn-Sham eigenvalues of $H^{0-{\rm QS}GW}$ rather than the complex quasiparticle energies, although the latter can in principle also be obtained.

To compare with optical properties and study the screening aspects, we have also calculated the macroscopic dielectric function $\varepsilon(\omega)$. The latter can be obtained in two ways. First, the dielectric response function matrix element

$$\varepsilon_{\mathbf{G}\mathbf{G}'}(\mathbf{q},\omega)=\sum_{IJ}\langle\mathbf{q}+\mathbf{G}|M_I\rangle[1-v\Pi^0(\mathbf{q},\omega)]_{IJ}\langle M_J|\mathbf{q}+\mathbf{G}'\rangle, \tag{1}$$

in a plane wave basis set,

$$\langle\mathbf{r}|\mathbf{q}+\mathbf{G}\rangle=\frac{1}{\sqrt{\Omega}}e^{i(\mathbf{q}+\mathbf{G})\cdot\mathbf{r}}, \tag{2}$$

can be obtained from the mixed basis set $|M_I\rangle$ matrix representation of $\Pi^0(\mathbf{q},\omega)$. Without local-field effects, we then have

$$\varepsilon^{\rm NLF}(\omega)=\lim_{\mathbf{q}\to0}\varepsilon_{00}(\mathbf{q},\omega) \tag{3}$$

while, with local field effects,

$$\varepsilon^{\rm LF}(\omega)=\lim_{\mathbf{q}\to0}\frac{1}{\varepsilon_{00}^{-1}(\mathbf{q},\omega)}. \tag{4}$$

Note that these quantities can be obtained for the LDA Hamiltonian as well as the QSGW Hamiltonian. To determine the limit for $\mathbf{q}\to0$, we simply take a finite small **q** value. However, care must be taken here not to take **q** too small

because the latter exhibits unphysical poles at high energy which influence the real part at lower energies by Kramers-Kronig transformation.

Second, one can take the limit of $\mathbf{q} \to 0$ analytically by transforming to the Adler-Wiser form:

$$\varepsilon_2(\omega) = \frac{8\pi^2 e^2}{\Omega\omega^2} \sum_n \sum_{n'} \sum_{\mathbf{k}\in BZ} f_{n\mathbf{k}}(1 - f_{n'\mathbf{k}}) \times |\langle\psi_{n\mathbf{k}}|[H,\mathbf{r}]|\psi_{n'\mathbf{k}}\rangle|^2 \delta(\omega - \epsilon_{n'\mathbf{k}} + \epsilon_{n\mathbf{k}}). \quad (5)$$

Here we give the expression for the imaginary part $\varepsilon_2(\omega)$ and the matrix elements entering the equation are strictly speaking those of the velocity operator $\dot{\mathbf{r}} = (i/\hbar)[H,\mathbf{r}]$ but are usually transformed to those of the momentum operator $\mathbf{v} = \mathbf{p}/m$. This however is no longer correct when a nonlocal potential is present. To correct for this we use the approximation proposed by Levine and Allan [43], which consists of rescaling the matrix elements by a factor $(\epsilon_{n'\mathbf{k}} - \epsilon_{n\mathbf{k}})/(\epsilon^{\mathrm{LDA}}_{n'\mathbf{k}} - \epsilon^{\mathrm{LDA}}_{n\mathbf{k}})$. The advantage of this formulation is that the separate contributions of each band pair and $\mathbf{k}$ point can be determined and secondly, the difficulty with taking the $\mathbf{q} \to 0$ limit are avoided.

The optical matrix elements of the momentum operator in the FP-LMTO method are calculated using the same "threefold representation" as used for the kinetic energy, potential, etc. The integral is determined first using the smooth envelope function part of the muffin-tin orbitals over the unit cell using a fast Fourier transform (FFT) method. Then the spherical harmonic expansion in each sphere of the envelope functions is subtracted and replaced by the integrals with the augmented functions. Actually the threefold procedure is applied to the symmetrized and already modulo-squared contributions of the matrix element. Explicitly we can write

$$|\langle\chi_i|p_\alpha|\chi_j\rangle|^2 = |\langle\tilde{\chi}_i|p_\alpha|\tilde{\chi}_j\rangle|^2 + \sum_{\mathbf{R},LL'kk'} C^{(i)*}_{\mathbf{R}Lk} C^{(i)}_{\mathbf{R}L'k'} \times[|\langle P_{\mathbf{R}Lk}|p_\alpha|P_{\mathbf{R}L'k'}\rangle|^2 - |\langle\tilde{P}_{\mathbf{R}Lk}|p_\alpha|\tilde{P}_{\mathbf{R}L'k'}\rangle|^2] \quad (6)$$

in which p_α is the αth Cartesian component of the momentum operator, $\tilde{\chi}_i$ is the ith envelope function, and χ_i its augmented muffin-tin orbital. Likewise, $\tilde{P}_{\mathbf{R}Lk}$ is the polynomial times spherical harmonic expansion $[\tilde{P}_{\mathbf{R}Lk} = p_{kl}(r_{\mathbf{R}})Y_L(\hat{r}_{\mathbf{R}})]$ of angular momentum $L = l,m$ and polynomial order k of the envelope function in site $\mathbf{R}$ and the corresponding function without a tilde is the augmentation inside that sphere in terms of ϕ and $\dot{\phi}$ that matches each polynomial in value and slope. The expansion coefficients $C^{(i)}_{\mathbf{R}Lk}$ provide the amount of each augmentation channel in each sphere present in the envelope function. Because of the imperfect cancellation between the smooth part calculated on a mesh and its spherical harmonic expansion, this can artificially lead to small negative values of the matrix element squared, which is unphysical but has no great consequences as long as we keep the augmentation in the spheres sufficiently well converged.

III. RESULTS

A. Bulk and monolayer band structures in the LDA

In this subsection we first revisit the basic electronic band structure of V_2O_5 at the LDA level, and, in particular, discuss the orbital character of the bands. Figure 2 shows an overview of the energy bands of V_2O_5 along symmetry lines in the standard Brillouin zone as defined in Ref. [44] for the orthorhombic Bravais lattice. The Brillouin zone nomenclature is shown in Fig. 3. Figure 2 also shows the corresponding density of states decomposed in various partial contributions. The zero is placed at the valence band maximum (VBM).

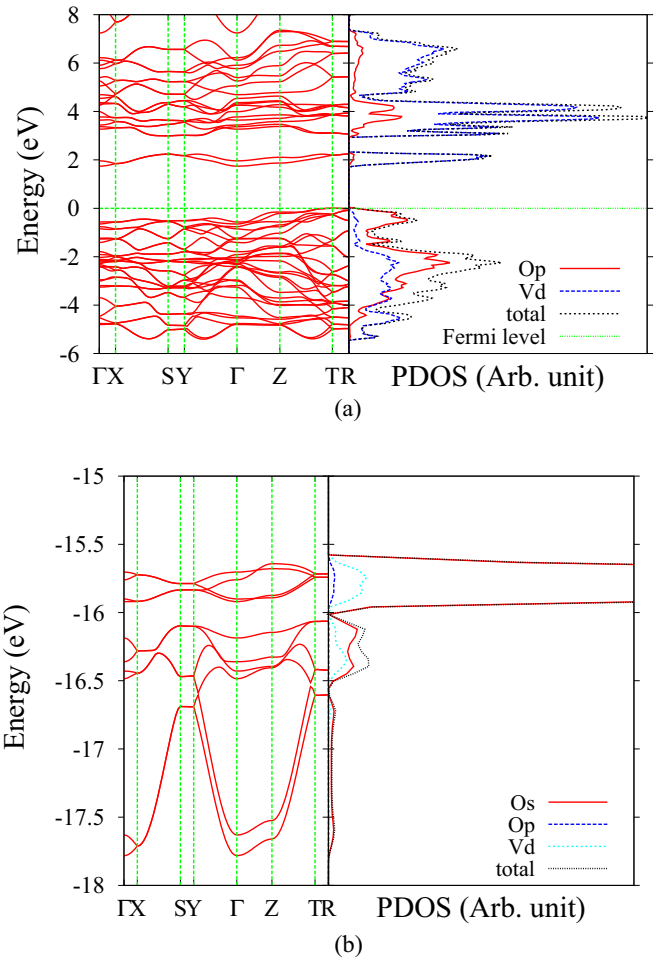

FIG. 2. (Color online) Overview band structure of V_2O_5 in LDA. Left: Bands along symmetry lines defined in Fig. 3. Right: Density of states decomposed various partial densities of states. Top panel (a): main O-2p valence and V-3d derived conduction bands. Bottom panel (b): lower O-2s derived bands.

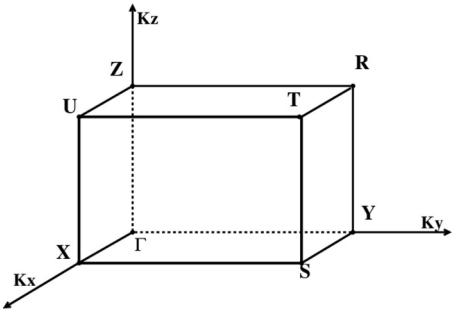

FIG. 3. Brillouin zone labeling of high-symmetry points.

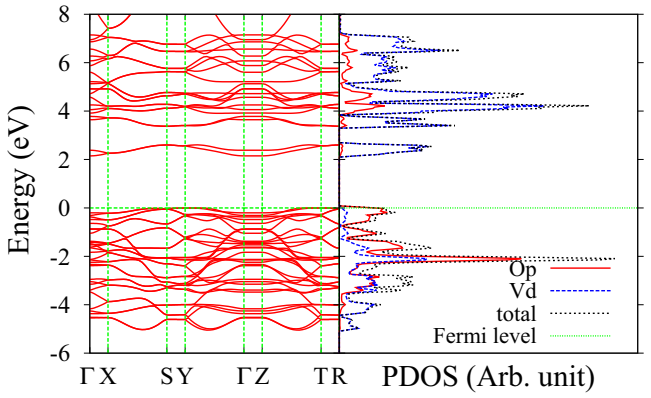

FIG. 4. (Color online) Energy bands in monolayer V_2O_5 in LDA for a monolayer spacing of $L = 18.66$ Å.

The bands between -18 and -15.5 eV are the O-2s derived bands, the bands between -6 an 0 eV are the mainly O-2p derived valence bands. The V-3p semicore states are not shown but lie at about -22 eV below the VBM. The highest set of valence bands also contain some V-3d contribution as they are bonding states of O-2p and V-3d. The lower conduction bands are mainly V-3d derived and show the split-off band mentioned already in the Introduction. The V-3d band extends till about 7 eV above the VBM. At higher energies we find the V-4s derived bands. The gap is seen to be indirect between a valence band maximum (VBM) near the point T and the conduction band minimum (CBM) at Γ. The indirect minimum gap is 1.74 eV (at T-Γ) while the lowest direct gap at (at Γ) is 2.30 eV. We note the degeneracies at the Brillouin zone edges which are related to the nonsymmorphic nature of the space group P_{nma}.

We can see that in spite of the layered nature of the material, there is a substantial dispersion of the bands in the z direction near the top of the VBM. See, e.g., the bands along Γ-Z. In the monolayer, as shown in Fig. 4, the bands along Γ-Z become flat and the VBM becomes the same near Y as near R or T. This reduces the valence bandwidth by about 0.6 eV and opens the band gap correspondingly. This is evidence that there is some hopping between the layers in bulk. In fact, the shortest distances between O atoms in different layers occur between up-pointing O_v and the O_b in the layer on top. We find that both the O_v-p_x and O_b-p_z have strong contributions to the bands near T at the VBM and thus we conclude it is the hopping between these orbitals that is responsible for this dispersion. This can be seen in Fig. 5. In Fig. 5 and other similar figures, the thin red lines are the bands, the color represents the intensity of a "spectral function" $A_i(\mathbf{k},\epsilon) = \sum_n |\langle \chi_i^{\mathbf{k}} | \psi_n^{\mathbf{k}} \rangle|^2 \delta(\epsilon - \epsilon_{n\mathbf{k}})$ with basis-set orbital i summed over all $(\kappa, R_{\rm sm})$ for a given angular momentum and site. The δ function is broadened by a Gaussian. Our reason for presenting the orbital character in this manner is that it allows us to visualize even small orbital contributions to each band, not only the dominant orbital character.

Now we address the orbital character in the conduction bands in more detail. We can see from the V-d_{xy} weighted band structure in Fig. 6 that the split-off band and the lowest two

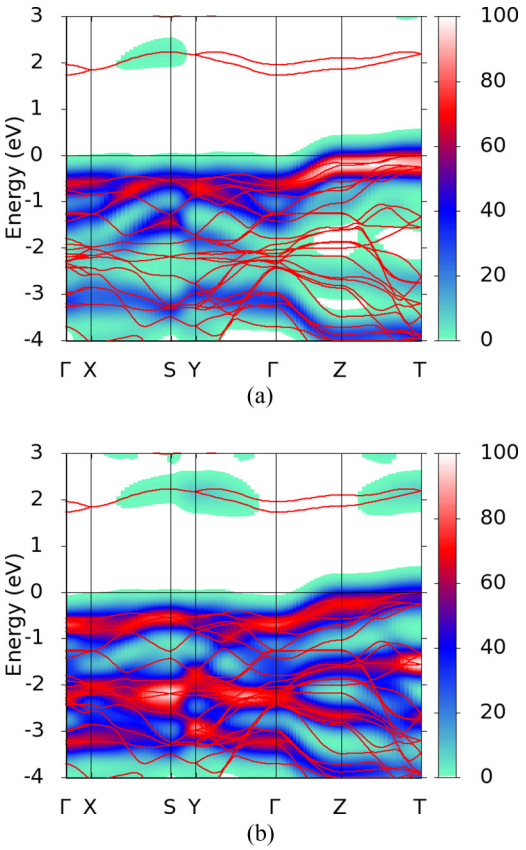

FIG. 5. (Color online) Valence bands weighted by (a) O_b-p_z and (b) O_v-p_x. See text for explanation of the color scheme.

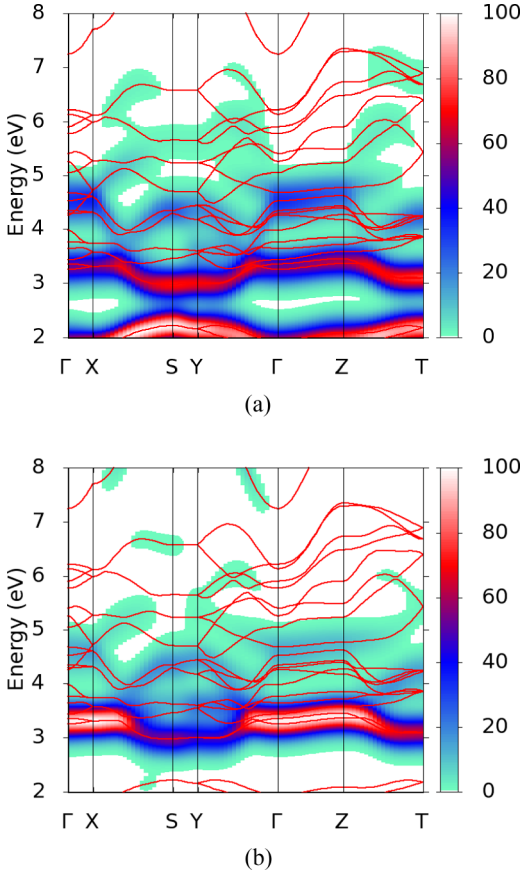

FIG. 6. (Color online) Lowest conduction bands of V_2O_5 weighted by (a) V-d_{xy} and (b) O_b-p_y.

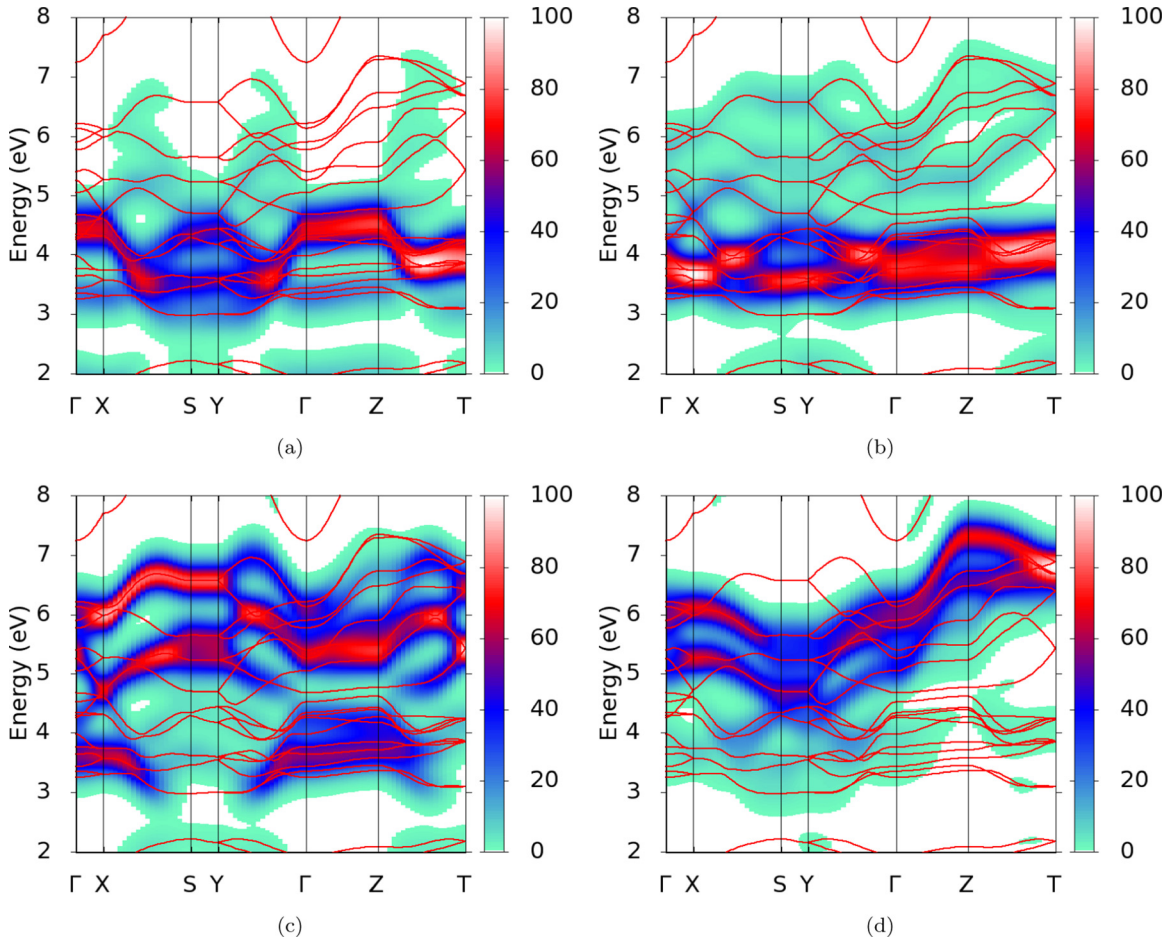

FIG. 7. (Color online) Vanadium 3d-derived conduction bands weighted by various d orbitals: (a) d_{yz}, (b) d_{xz}, (c) $d_{x^2-y^2}$, and (d) $d_{3z^2-r^2}$.

bands connected to the main set of conduction bands have d_{xy} character. Further analysis shows that the split-off band has no O_b-p_y character while the next two do. The split-off bands, in fact, are antisymmetric with respect to the mirror plane passing through O_b and thus cannot couple to the O-p_y. This confirms the nature of the split-off conduction band as discussed already in the Introduction and well known since Refs. [4,5].

Projections on other V-3d orbitals show their weight throughout the conduction band range. See Fig. 7. As expected, the t_{2g}-like yz and zx orbitals, which have π antibonding character with the O-2p lie near the bottom of the main set of conduction bands (not counting the split-off band), while the e_g-like orbitals x^2-y^2 and $3z^2-r^2$ contribute more to the bands at higher energy because of their stronger σ-antibonding character. In particular the highest bands correspond to $3z^2-r^2$ which points toward the closest O_v in the z direction.

B. Bulk band structure and optical properties in QSGW

In this subsection we discuss the QSGW bands of bulk V_2O_5. In Fig. 8 we show the band structure of V_2O_5 calculated using the QSGW method and with the zero placed at the VBM as usual.

The band gaps, bandwidths, and other band structure overview properties are summarized in Table II compared to LDA and experiment. We can see that the O-2s derived bands shift down by 1.75 compared to the VBM. The O-2p valence bandwidth is increased by 0.67 eV. Thus we find that the further we shift down from the VBM, the larger the self-energy correction. The lowest indirect and direct gap shift by 2.26 and 2.53 eV, respectively, showing some **k** dependence of the gap correction. The split-off band separation from the main conduction bands changes by only 0.1 eV. The

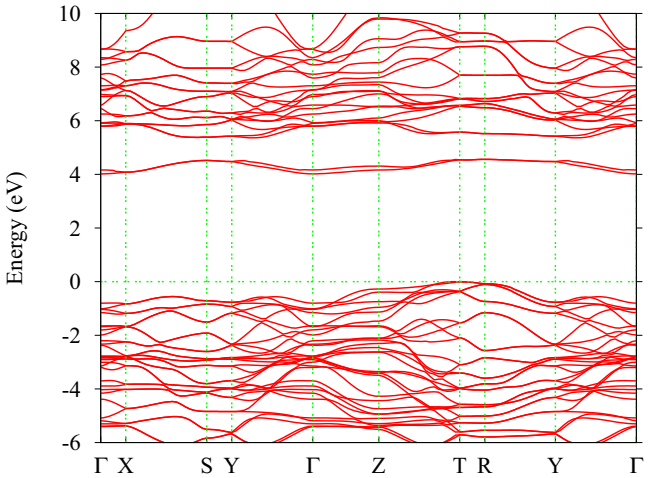

FIG. 8. (Color online) Energy bands of bulk V_2O_5 in the QSGW method.

TABLE II. Various V_2O_5 band structure characteristics in different models and experiment.

	LDA	QSGW	Expt.	0.38$\Delta\Sigma$
Indirect gap (T-Γ)	1.74	4.0		1.98
Lowest direct gap at Γ	2.30	4.83	2.35 ± 0.01[a]	2.60
Split-off band separation	0.76	0.86		0.88
O-2p valence bandwidth	5.39	6.06	5.5 ± 0.5[b]	5.79
DOS peak of O-2s bands from VBM	–15.7	–18.5	–17.6[c]	–16.84
V-3d bandwidth	5.80	5.80		4.75

[a]Reference [45].
[b]Reference [46].
[c]In Ref. [47] the O-2s measured by XPS is found at 20 eV below the Fermi level, which in turn we estimate is 2.4 eV above the VBM near the CBM.

most notable feature in the table is that the QSGW strongly overestimates both the direct and indirect gaps. QSGW is known to overestimate gaps systematically. However, for most tetrahedral semiconductors the overestimate is only by about 20% and is ascribed to the random phase approximation (RPA) underestimate of the screening in calculating W.

Before we discuss the comparison of the calculated gap with experiment, it is necessary to discuss the experimental data. The optical absorption spectra measured by Hevesi [48] and Kenny *et al.* [45] both show an exponential onset or Urbach tail. This is associated with defect states below the gap. Kenny *et al.* [45] showed a good fit of the absorption edge in the region above the absorption tail to an equation of the form $Kh\nu \propto (h\nu - E_g)^{3/2}$, which was interpreted as direct forbidden transitions. The gap extracted this way is 2.36 eV for $\mathbf{E} \parallel \mathbf{a}$ and 2.34 eV for $\mathbf{E} \parallel \mathbf{b}$. (Note that they interchange **b** and **c** axes from ours.) We thus can place the smallest direct gap to be compared with our gap at Γ at 2.35 ± 0.01 eV. This is remarkably close to our LDA gap, indicating that the QSGW gap is significantly overestimated. While a slight overestimate (of order a few 0.1 eV) of the gaps by QSGW is typically observed in semiconductors, the overestimate here is much larger, 2.5 eV.

To further scrutinize this interpretation as a direct forbidden transition, we have determined the symmetry of the states near the VBM and CBM at Γ by inspecting the eigenvectors. The VBM at Γ has symmetry A_{1g}, the VBM $-$ 1 has symmetry B_{2u}, the CBM at Γ has symmetry B_{3u}, and the CBM + 1 has symmetry B_{1g} using the D_{2h} point group and the notation of Tinkham [49]. This means the lowest direct transition is actually allowed for $\mathbf{E} \parallel \mathbf{a}$. If we insist on using $K \propto (h\nu - E_g)^{1/2}$ as expected for direct allowed transitions, then the plots of Kenny *et al.* [45] show a less good fit, which may just mean that the Urbach tail extends to higher energies and extrapolating the higher part of these curves we obtain a gap of about 2.45 eV for $\mathbf{E} \parallel \mathbf{a}$. So, perhaps, we rather should say the direct gap is at 2.40 ± 0.05 eV.

Instead of just comparing with the quoted gap values, we also compare our calculated optical dielectric function directly with experimental data from spectroscopic ellipsometry by Parker *et al.* [26]. In Fig. 9 we compare the measured dielectric function $\varepsilon_2(\omega)$ with calculations for LDA and 0.38$\Delta\Sigma$. The

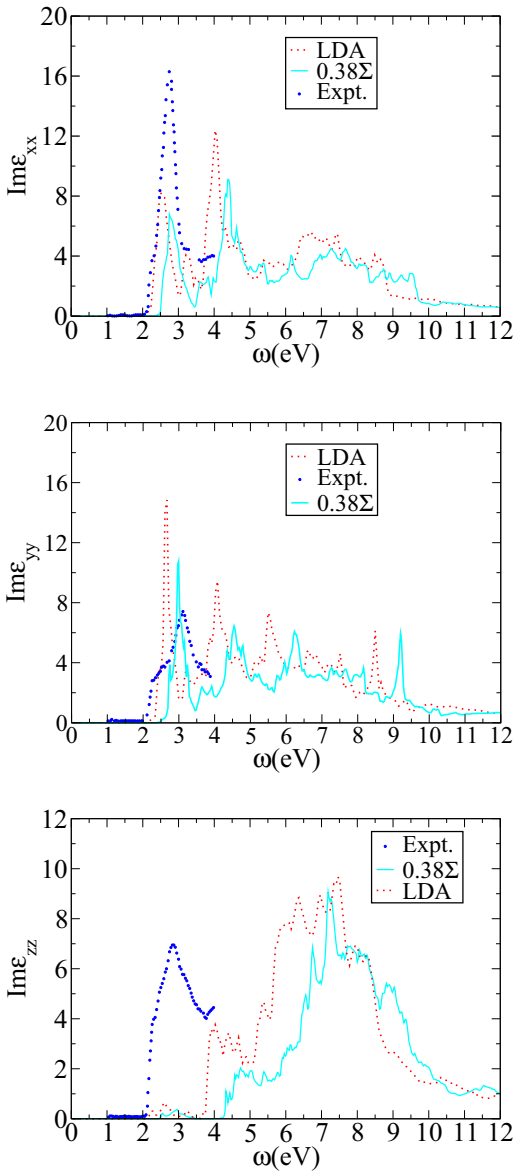

FIG. 9. (Color online) Comparison of calculated $\varepsilon_2(\omega)$ in various approximations with experiment. From top to bottom, xx, yy, and zz components. In each case we compare Expt., LDA, and 0.38$\Delta\Sigma$.

origin of the reduction factor is discussed below. We note that our LDA results differ somewhat from the LDA calculations presented by Parker *et al.* [26] because of the use of different band structure methods. Because of the anisotropy we need to distinguish the ε_{xx}, ε_{yy}, and ε_{zz} components. (Again, note that our **b** and **c** are switched from theirs.) These dielectric functions were calculated using the Adler-Wiser approach.

We can see that the first peak matches rather well in both x and y direction although the onset or minimum gap seems to be a bit overestimated. The experimental result seems to strongly overestimate the z polarized $\varepsilon_2(\omega)$. This was also the case for the LDA results of Parker *et al.* [26]. This may be related to experimental difficulties in measuring the $\mathbf{E} \parallel \mathbf{c}$ component. In fact, Parker *et al.* [26] mention that all measurements are done on ab planes, so the latter are obtained from differences between two incident angles which however were chosen

rather close to each other instead of using nearly normal and nearly glancing incidence.

Before addressing the overestimate of the QSGW gap we must make sure that this does not simply arise from a confusion between the fundamental quasiparticle gap and the optical gap. The fundamental gap is defined as the difference between ionization potential and electron affinity as measured, respectively, by photoemission and inverse photoemission. Remarkably, such data are in fact available [50] for V_2O_5 and give a gap of 2.8 eV. This is about 0.4 eV higher than the optical gaps but there is unfortunately a larger uncertainty on these data because of the limited resolution of these spectroscopies and the uncertainties on the position of the Fermi level in oxygen deficient V_2O_5 which could have its Fermi energy in the split-off band or below it in oxygen vacancy derived levels. Thus we do not consider this as evidence for a 0.4 eV exciton binding energy. In fact, the optical spectra shown in Fig. 9 do not feature a prominent sharp exciton, nor a Rydberg series of excited states of the exciton, but rather a straightforward absorption edge representative of interband transitions. It clearly shows, however, that a fundamental direct gap $E_g > 4$ eV as obtained in QSGW is incompatible with photoemission and inverse photoemission data.

Another approach to this question is by comparing photoemission in V_2O_5 with that in reduced oxides, such as V_6O_{13}. Essentially in V_6O_{13} one expects the lowest conduction band of V_2O_5 to be partially filled in addition to having oxygen vacancy related states. Such measurements [46] indeed show an additional feature in photoemission related to the V-3d occupied bands with a well defined Fermi edge. The V_2O_5 like O-2p dominated valence band edge lies indeed about 2.5 eV below the Fermi edge in V_6O_{13}. Unfortunately the resolution of photoemission is not sufficient to determine the gap precisely. However, it does show these measurements are compatible with a fundamental gap of about 2.5 eV rather than >4 eV as predicted by QSGW. Even if one were to interpret these shifts between the fundamental gap between one-particle states and the optical gap as evidence of excitonic or electron-hole interaction effects, they are seen to be only of order 0.3–0.4 eV. This also suggests that the electron-hole interaction effects on W are of the same order of magnitude and cannot explain the main discrepancy with the QSGW result.

Our QSGW results are consistent with the findings by Lany [28] although he used a different GW^{RPA} approach. He started from GGA + U (generalized gradient approximation with Hubbard-U correction) calculations and iterated only the eigenvalues in the G in his GW^{RPA} approach while keeping W fixed at the initial RPA level calculation. The gap reported in his paper is 4.69 eV, in fact, rather close to our 4.83 eV for the direct gap at Γ in QSGW although it was not specified whether his result refers to the direct or indirect gap. To overcome this discrepancy, he suggested adding an additional downward shift of the V-3d states for both occupied and empty states by means of an external potential. This approach, however, lacks first-principles justification. Instead we propose to reduce the $\Delta\Sigma$ by a correction factor representing the increase in screening for reasons explained below.

We now address the reason for the large required reduction of $\Delta\Sigma$. It has recently been pointed out that for ionic materials, the lattice contribution to the polarization entering GW calculations can be substantial [31,32,51]. The general effect is known since early work of Fowler [52] and Kunz [53]. Recently its implications have been revisited in the context of GW calculations [31]. It is important to distinguish this macroscopic "polaronic" contribution to the polarizability from the usual gap correction from the electron-phonon interaction, whose effect is generally small. While Bechstedt [31] already laid out the frequency dependent formalism for including the lattice polarization effect in GW calculations, in the end he took into account that the lattice polarization effect should die out at frequencies substantially above the LO frequencies and hence took into account only the static modification of the long-range macroscopic dielectric constant for the statically screened contributions to the self-energy. The same approach was followed by Vidal *et al.* [51]. Botti and Marquez [32] were the first to fully include the frequency dependent modifications.

More specifically, for a polar material, the lattice LO phonon modes lead to an increase in the dielectric constant even at finite frequencies,

$$\varepsilon^{\alpha}_{\mathrm{tot}}(\mathbf{q}\to 0,\omega) = \varepsilon^{\alpha}_{\mathrm{el}}(\mathbf{q}\to 0,\omega)\prod_i \frac{\omega^2_{\mathrm{LO}i}-\omega^2}{\omega^2_{\mathrm{TO}i}-(\omega+i0^+)^2}, \quad (7)$$

where the product is over all modes i corresponding to the Cartesian direction α. This effect is expected to be significant in V_2O_5 because the ratio of the static (including phonon contributions) to high-frequency (i.e., electronic screening only) dielectric constants $\varepsilon^{\alpha}_0/\varepsilon^{\alpha}_{\infty}$ at zero frequency are as large as 4.00, 3.62, and 1.25 for $\alpha \parallel \mathbf{a}, \mathbf{b}, \mathbf{c}$, respectively [23]. Including the anisotropy and frequency dependence properly in the QSGW calculation is beyond the scope of this paper. Since we currently do not have an easy way to split the Σ into a static and dynamic part, we simply assume the static part is dominant. This is justified somewhat by the success of the statically screened exchange approximation. For simplicity we then apply the correction factor due to the lattice polarization to the whole Σ rather than the static part only. A simple way to average over the directions is

$$\frac{\Sigma_{\mathrm{tot}}}{\Sigma_{\mathrm{el}}} = \frac{W_{\mathrm{tot}}}{W_{\mathrm{el}}} \approx \left(\frac{\varepsilon^a_{\infty}\varepsilon^b_{\infty}\varepsilon^c_{\infty}}{\varepsilon^a_0\varepsilon^b_0\varepsilon^c_0}\right)^{1/3}. \quad (8)$$

This will clearly overestimate the effect because in reality the correction factor of $\varepsilon(\omega)$ should have died out for $\omega \gg \omega_{\mathrm{LO}}$. Thus our approach ignores the details of the frequency dependence and anisotropy averaging near $\mathbf{q}\to 0$ but still allows us to roughly estimate the degree of reduction by lattice polarization. Using the data for the static and high-frequency dielectric constants calculated in our previous paper [23], we obtain $\Sigma_{\mathrm{tot}} = 0.38\Sigma_{\mathrm{el}}$. Using $0.38\Delta\Sigma$ we obtain a direct gap of 2.6 eV.[1] We expect our estimate to be an overestimate of the effect so the gap after modification by the lattice polarization effect should still be larger than 2.6 eV. The remainder might then be attributed to the orbital dependent electron-hole ladder diagrams affecting the screening mentioned earlier.

The origin of the large $\varepsilon_0/\varepsilon_{\infty}$ factors in V_2O_5 can further be traced to specific phonons using the generalized Lyddane-

[1] By scaling $\Delta\Sigma = \Sigma - v^{\mathrm{LDA}}_{\mathrm{xc}}$ by a correction factor instead of only Σ, the overestimate of the effect is somewhat reduced.

Sachs-Teller relation. As can be seen in Ref. [23], Table I, the modes primarily contributing to this factor for the the x component along **a** are the $B_{3u}^{(3)}$, $B_{3u}^{(4)}$, and $B_{3u}^{(5)}$ modes which give $(\omega_{\rm LO}/\omega_{\rm TO})^2$ factors of 1.52, 1.94, and 1.28, respectively. These correspond to the broad Reststrahlen bands seen in Fig. 2 of Ref. [23]. Similarly for the **b** direction, there is only one mode $B_{2u}^{(3)}$ with a large $(\omega_{\rm LO}/\omega_{\rm TO})^2$ of 2.77. We note further that this corresponds to a vibrational motion along the chain direction in which the V-O_b-V rungs move against the O_c and hence lead to a strong bond stretch of the V-O_c along the chain and corresponding dipole. The B_{3u} modes leading to the enhancement of ε^a correspond to V-O_b stretch modes or motions of one chain with respect to the other. We note that the in-plane enhancement of ε is much stronger than perpendicular to the plane, where mostly the $B_{1u}^{(6)}$ mode corresponding to the V-O_v stretch provides a $(\omega_{\rm LO}/\omega_{\rm TO})^2$ factor of 1.15.

C. Monolayer band structure and dielectric constants in QSGW

Having understood the limitations of QSGW for the bulk of V_2O_5 we now move on to the monolayer. The band structures of the monolayer were determined at the QSGW level for different interlayer spacings L. More precisely L is defined as the size of the unit cell in the **c** direction perpendicular to the layers. First of all, we show the band structure of the monolayer in QSGW for the layer spacing $L = 11.512$ Å in Fig. 10.

We can see that the location of the VBM is different from bulk. Although the VBM is rather flat between $RTSY$ we find the VBM to occur about halfway between Y and Γ. The fact that the bands along Γ-Z are flat and the bands in the $ZRTU$ plane are almost indistinguishable from those in the ΓYSX indicates that the layer separation is sufficient to avoid band dispersion.

Second, we find that the gap converges very slowly with L. As can be seen in Fig. 11 the QSGW gap correction beyond LDA varies linearly as a function of $1/L$. The extrapolated gap for $L \to \infty$ is as large as 7.66 eV with full QSGW. Clearly the $1/L$ dependence of the gap is a result of the long-range terms in Σ, that is the screened exchange term.

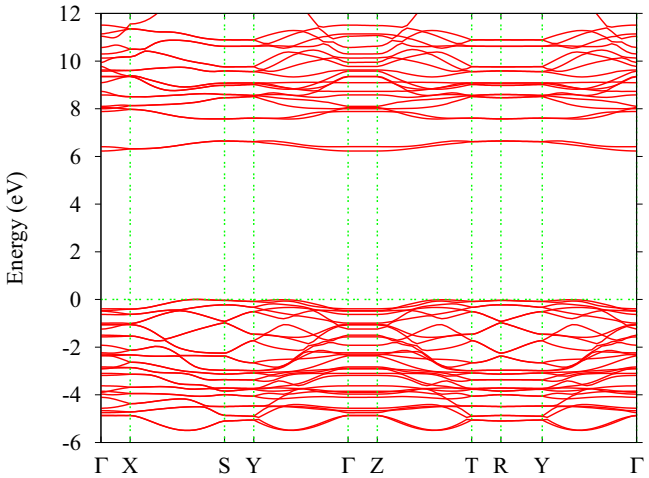

FIG. 10. (Color online) Band structure of monolayer V_2O_5 with interlayer spacing $L = 11.512$ Å in the QSGW method.

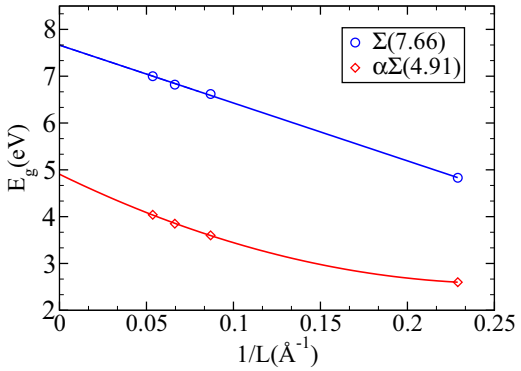

FIG. 11. (Color online) Direct band gap of V_2O_5 monolayer as a function of $1/L$ with L the interlayer spacing. The circles and blue line give the QSGW results without lattice polarization correction, the diamonds and red lines give the results including the lattice polarization correction, assuming $\alpha = \varepsilon_\infty/\varepsilon_0$ also vary as $1/L$. Here $\alpha = 0.38$ for bulk and 0.49, 0.51, and 0.52 for monolayer with increasing L, respectively. The numbers in parentheses give the extrapolated gap for $L \to \infty$.

The electronic dielectric constants were also calculated as a function of L. In Table III we give dielectric constants calculated using the Adler-Wiser approach and Kramers-Kronig transformation based on the LDA bands as well as those with the $0.38\Delta\Sigma$ model for bulk and compare them to experimental results and our previous calculation using the linear response approach with a plane wave method [23]. We found the finite **q** approach to be less accurate because of the problem of avoiding high-frequency pole contributions while at the same time approaching $\mathbf{q} \to 0$ sufficiently closely. We note that with full QSGW, the dielectric constants are significantly underestimated as expected because of the gap overestimate. We note that the closest agreement with experiment occurs for the reduced Σ model.

TABLE III. High-frequency dielectric constant in V_2O_5 as a function of layer spacing.

L (Å)	ε_{xx}	ε_{yy}	ε_{zz}
4.38	5.48[a]	5.25[a]	4.63[a]
Bulk	4.35[b]	4.13[b]	3.49[b]
	6.54[c]	6.08[c]	3.87[c]
	4.28[d]	4.49[d]	3.88[d]
	7.29[e]	6.00[e]	4.28[e]
11.512	2.60[a]	2.54[a]	2.24[a]
	2.97[c]	2.75[c]	1.43[c]
15.084	2.23	2.17	1.95
18.656	2.00	1.95	1.77

[a]This work, LDA using Adler-Wiser formula and Kramers-Kronig transformation.
[b]This work, $0.38\Delta\Sigma$ using Adler-Wiser formula and Kramers-Kronig transformation.
[c]Using *ab initio* LDA plane wave pseudopotential calculation by Bhandari *et al.* [23].
[d]From refractive index in the wavelength range (0.6708–0.5893 μm) extrapolated to $\lambda \to \infty$ of V_2O_5 single crystal by Kenny *et al.* [45].
[e]From refractive index at $\lambda = 0.671$ μm, Clauws *et al.* [54].

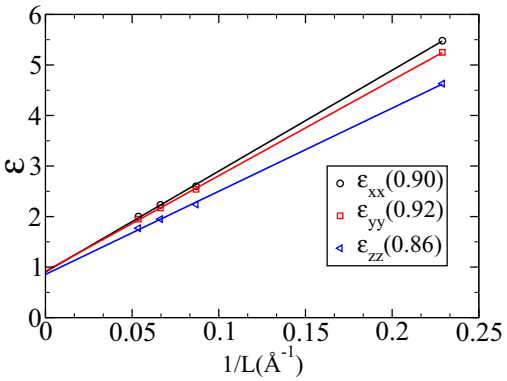

FIG. 12. (Color online) Real part of the electronic dielectric constant $\varepsilon_1(\omega = 0)$ (the values inside the bracketed are for $L = \infty$) of V_2O_5 as a function of $1/L$ with L the layer spacing calculated in LDA.

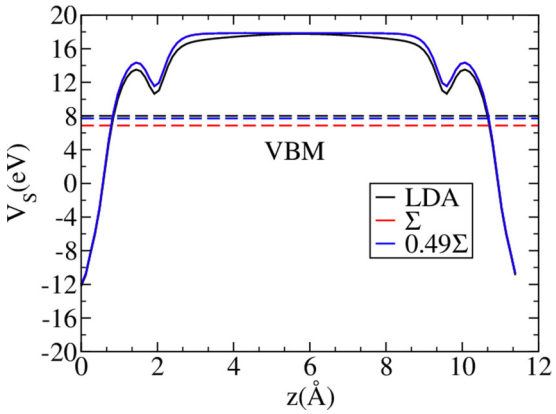

FIG. 13. (Color online) Smooth electrostatic potential (V_S) for monolayer V_2O_5 as a function of z, the distance normal to the layer and valence band maximum (dashed line) obtained within LDA, QSGW, and $0.49\Delta\Sigma$, giving ionization potentials of 9.7, 10.9, and 10.1 eV, respectively. The flat region corresponds to the vacuum reference level.

The dielectric constants are shown in Fig. 12 plotted as a function of $1/L$. Clearly these also behave linearly in $1/L$ as predicted by Cudazzo *et al.* [55]. This is a result of the strongly modified screening in a 2D system. All components extrapolate essentially to $\varepsilon \to 1$ for $L \to \infty$. The slope is opposite in sign to that of the gap as expected because the gap correction is proportional to Σ which in turn is proportional to W and hence to ε^{-1}.

In the previous section we have shown that QSGW overestimates the gap for the bulk and thus we expect this also to be the case for the monolayer. We apply the lattice polarization effect in the same approximate way as in Eq. (7) by a simple reduction factor. However, the $\varepsilon^{\alpha}_{\infty}/\varepsilon^{\alpha}_{0}$ factors are different for the monolayer and for the bulk. We assume that they also vary linearly as $1/L$ and use the results of Ref. [23] to find the correction factor for each L. The gaps obtained in this way are shown in Fig. 11. Because both the QSGW and the lattice polarization factor have the form of a constant plus a $1/L$ term, the final result is fitted to a quadratic equation $A + B/L + C/L^2$, giving the full-line interpolation through the points and leading to a final predicted fundamental gap for the monolayer of 4.91 eV. We emphasize that this is the fundamental quasiparticle gap because excitonic effects may also be expected to be stronger in the monolayer and could reduce the optical gap. We note that if instead, as Lany [28] suggested, we had applied a simple d band shift, the QSGW results without lattice effect would have simply shifted down by 3.4 eV but with the same slope. This would have given a significantly larger gap of 5.57 eV.

Another interesting point is that from the monolayer calculation we can extract an ionization potential or work function. In fact, we can plot the smooth part of the electrostatic potential relative to the internal zero used in the calculation and place the VBM relative to this same zero. This is shown in Fig. 13. This gives us a calculated work function of 9.7 eV in LDA and including the absolute QSGW shift, 10.9 eV in QSGW, or after including the lattice polarization effect (reduction factor 0.49 for a monolayer), 10.1 eV. Experimentally the work function of a V_2O_5 (001) surface was measured by Grymonprez *et al.* [56]. It was found to be 6.71 eV for a freshly cleaved surface. The question, however, is whether this corresponds to the VBM which is nominally the highest occupied state or to the CBM, which one might assume to be slightly filled if there is some doping present from oxygen vacancies or impurities. In Ref. [56] it was also found that after electron bombardment, the ionization potential shifted down by about 0.6 eV. This would correspond to further filling of the conduction band. This shift certainly is much smaller than the gap and thus indicates that even on a fresh surface, the work function measured already determines a Fermi level close to the conduction band edge rather than the valence band edge. With this interpretation, the VBM would correspond to an ionization potential of about 9.0 eV assuming a gap of about 2.3 eV. Recently a very high ionization potential of 9.5 eV was reported for V_2O_5 along with a high work function of 7 eV and a Fermi level close to the conduction band minimum [50].

This seems to indicate that QSGW (10.9 eV) overestimates the ionization potential by about 1.5–2.0 eV which is somewhat larger than what is found for most semiconductors by Grüneis *et al.* [57]. We note that the size quantization effects in a monolayer are expected to shift up the electron states and hence reduce the ionization potential compared to that near a surface of a bulk crystal. Thus the discrepancy may be even larger. The result including lattice polarization or LDA appear to be closer to experiment.

IV. CONCLUSIONS

In this paper we first discussed some reasons why it is of interest to study the monolayer V_2O_5 electronic band structure. We summarized the interesting features of the band structure at the LDA level. Band structures calculated at the QSGW level were presented. After a careful review of the experimental literature data, the QSGW was shown to overestimate the band gap significantly more than is usual for sp-bonded semiconductors. We identified the lattice polarization as the major missing ingredient responsible for this discrepancy. A rough estimate of this effect in the form of an overall reduction factor of $\Delta\Sigma$ based on the previously calculated dielectric constants with

and without the lattice polarization, led to a reduction factor of 0.38. Including this factor, we obtain fair agreement between our calculated imaginary part of the dielectric function with spectroscopic ellipsometry data. We expect our lattice polarization effect to be slightly overestimated by our simplified static approximation and hence part of the discrepancy on the gap must still result from other not included effects, such as missing electron-hole diagrams in the calculation of W. In any case, it was found that the gap overestimate is not due to a large bound exciton effect but rather already affects the quasiparticle fundamental gap. This is confirmed by the comparison of IPES-PES data with optical absorption and spectroscopic ellipsometry data in the literature.

The band gaps of the monolayer at the QSGW level were found to depend inversely on the layer spacing as $1/L$ and this was shown to originate from the long-range screened exchange term as the corresponding ε also shows a $1/L$ behavior. The latter also must be corrected by a different lattice polarization factor because the ratio of lattice to electronic screening itself is different in the monolayer from the bulk. In the end, our extrapolated results still predicts a significant increase of the fundamental quasiparticle gap of the free-standing monolayer from the bulk.

We also determined the ionization potential of the monolayer and found it to agree qualitatively with the reported high value of 9–10 eV and to be overestimated by QSGW by at least 1 eV as has also been observed for other materials in recent work.

ACKNOWLEDGMENTS

This work was supported by the Air Force Office of Scientific Research under Grant No. FA 9550-12-1-0441 (C.B.) and the US Department of Energy, Office of Science, Basic Energy Sciences, under Grant No. ER-46874-SC0008933 (W.L.). M.v.S. thanks the Simons foundation for financial support with their collaboration on the many-electron problem. The calculations were preformed at the High Performance Computing Resource in the Core Facility for Advanced Research Computing at Case Western Reserve University.

[1] K. S. Novoselov, A. K. Geim, S. V. Morozov, D. Jiang, Y. Zhang, S. V. Dubonos, I. V. Grigorieva, and A. A. Firsov, Science **306**, 666 (2004).
[2] H. G. Bachmann, F. R. Ahmed, and W. H. Barnes, Z. Krist. **115**, 110 (1961).
[3] D. W. Bullett, J. Phys. C: Solid State Phys. **13**, L595 (1980).
[4] W. Lambrecht, B. Djafari-Rouahni, and J. Vennik, J. Phys. C: Solid State Phys. **14**, 4785 (1981).
[5] H. Smolinski, C. Gros, W. Weber, U. Peuchert, G. Roth, M. Weiden, and C. Geibel, Phys. Rev. Lett. **80**, 5164 (1998).
[6] L. Fiermans, P. Clauws, W. Lambrecht, L. VandenBroucke, and J. Vennik, Phys. Status Solidi A **59**, 485 (1980).
[7] G. Bauer, V. Güther, H. Hess, A. Otto, O. Roidl, H. Roller, and S. Sattelberger, *Vanadium and Vanadium Compounds* (Wiley, Weinheim, 2005).
[8] J. Haemers, E. Baetens, and J. Vennik, Phys. Status Solidi A **20**, 381 (1973).
[9] P. Clauws and J. Vennik, Phys. Status Solidi B **66**, 553 (1974).
[10] M. Isobe and Y. Ueda, J. Phys. Soc. Jpn. **65**, 1178 (1996).
[11] K. Kobayashi, T. Mizokawa, A. Fujimori, M. Isobe, and Y. Ueda, Phys. Rev. Lett. **80**, 3121 (1998).
[12] S. Atzkern, M. Knupfer, M. S. Golden, J. Fink, A. N. Yaresko, V. N. Antonov, A. Hübsch, C. Waidacher, K. W. Becker, W. von der Linden *et al.*, Phys. Rev. B **63**, 165113 (2001).
[13] Z. S. Popović and F. R. Vukajlović, Phys. Rev. B **59**, 5333 (1999).
[14] H. Wu and Q.-q. Zheng, Phys. Rev. B **59**, 15027 (1999).
[15] S. Sorella and A. Parola, J. Phys.: Condens. Matter **4**, 3589 (1992).
[16] M. A. Korotin, I. S. Elfimov, V. I. Anisimov, M. Troyer, and D. I. Khomskii, Phys. Rev. Lett. **83**, 1387 (1999).
[17] V. Petkov, P. Y. Zavalij, S. Lutta, M. S. Whittingham, V. Parvanov, and S. Shastri, Phys. Rev. B **69**, 085410 (2004).
[18] G. T. Kim, J. Muster, V. Krstic, J. G. Park, Y. W. Park, S. Roth, and M. Burghard, Appl. Phys. Lett. **76**, 1875 (2000).
[19] J. Muster, G. T. Kim, V. Krsti, J. G. Park, Y. W. Park, S. Roth, and M. Burghard, Adv. Mater. **12**, 420 (2000).
[20] G.-m. Zhu, Z.-b. Qu, G.-l. Zhuang, Q. Xie, Q.-q. Meng, and J.-g. Wang, J. Phys. Chem. C **115**, 14806 (2011).
[21] A. D. Raj, P. S. Kumar, Q. Yang, and D. Mangalaraj, Physica E **44**, 1490 (2012).
[22] J. Bailey, G. Pozarnsky, and M. Mecartney, J. Mater. Res. **7**, 2530 (1992).
[23] C. Bhandari and W. R. L. Lambrecht, Phys. Rev. B **89**, 045109 (2014).
[24] V. Eyert and K.-H. Höck, Phys. Rev. B **57**, 12727 (1998).
[25] V. Brázdová, M. V. Ganduglia-Pirovano, and J. Sauer, Phys. Rev. B **69**, 165420 (2004).
[26] J. C. Parker, D. J. Lam, Y.-N. Xu, and W. Y. Ching, Phys. Rev. B **42**, 5289 (1990).
[27] A. Chakrabarti, K. Hermann, R. Druzinic, M. Witko, F. Wagner, and M. Petersen, Phys. Rev. B **59**, 10583 (1999).
[28] S. Lany, Phys. Rev. B **87**, 085112 (2013).
[29] H.-P. Komsa and A. V. Krasheninnikov, Phys. Rev. B **86**, 241201 (2012).
[30] M. van Schilfgaarde, T. Kotani, and S. Faleev, Phys. Rev. Lett. **96**, 226402 (2006).
[31] F. Bechstedt, K. Seino, P. H. Hahn, and W. G. Schmidt, Phys. Rev. B **72**, 245114 (2005).
[32] S. Botti and M. A. L. Marques, Phys. Rev. Lett. **110**, 226404 (2013).
[33] M. Methfessel, M. van Schilfgaarde, and R. A. Casali, in *Electronic Structure and Physical Properties of Solids. The Use of the LMTO Method*, Lecture Notes in Physics Vol. 535, edited by H. Dreyssé (Springer, Berlin, 2000), p. 114.
[34] T. Kotani and M. van Schilfgaarde, Phys. Rev. B **81**, 125117 (2010).
[35] W. Kohn and L. J. Sham, Phys. Rev. **140**, A1133 (1965).
[36] U. von Barth and L. Hedin, J. Phys. C **5**, 1629 (1972).
[37] http://www.lmsuite.org/
[38] ecalj package at https://github.com/tkotani/ecalj/. Its one-body part is developed based on Ref. [37].
[39] M. van Schilfgaarde, T. Kotani, and S. V. Faleev, Phys. Rev. B **74**, 245125 (2006).

[40] T. Kotani, M. van Schilfgaarde, and S. V. Faleev, Phys. Rev. B **76**, 165106 (2007).
[41] L. Hedin, Phys. Rev. **139**, A796 (1965).
[42] F. Aryasetiawan and O. Gunnarsson, Phys. Rev. B **49**, 16214 (1994).
[43] Z. H. Levine and D. C. Allan, Phys. Rev. Lett. **63**, 1719 (1989).
[44] C. J. Bradley and A. P. Cracknell, *The Mathematical Theory of Symmetry in Solids: Representation Theory for Point Groups and Space Groups* (Oxford University Press, Oxford, 1972).
[45] N. Kenny, C. Kannewurf, and D. Whitmore, J. Phys. Chem. Solids **27**, 1237 (1966).
[46] S. Shin, S. Suga, M. Taniguchi, M. Fujisawa, H. Kanzaki, A. Fujimori, H. Daimon, Y. Ueda, K. Kosuge, and S. Kachi, Phys. Rev. B **41**, 4993 (1990).
[47] L. Fiermans and J. Vennik, Surf. Sci. **24**, 541 (1971).
[48] I. Hevesi, Acta Phys. Acad. Sci. Hung. **23**, 415 (1967).
[49] M. Tinkham, *Group Theory and Quantum Mechanics* (McGraw-Hill, New York, 1964).
[50] J. Meyer, K. Zilberberg, T. Riedl, and A. Kahn, J. Appl. Phys. **110**, 033710 (2011).
[51] J. Vidal, F. Trani, F. Bruneval, M. A. L. Marques, and S. Botti, Phys. Rev. Lett. **104**, 136401 (2010).
[52] W. B. Fowler, Phys. Rev. **151**, 657 (1966).
[53] A. B. Kunz, Phys. Rev. B **6**, 606 (1972).
[54] P. Clauws and J. Vennik, Phys. Status Solidi B **76**, 707 (1976).
[55] P. Cudazzo, I. V. Tokatly, and A. Rubio, Phys. Rev. B **84**, 085406 (2011).
[56] G. Grymonprez, L. Fiermans, and J. Vennik, Surf. Sci. **36**, 370 (1973).
[57] A. Grüneis, G. Kresse, Y. Hinuma, and F. Oba, Phys. Rev. Lett. **112**, 096401 (2014).